ARTICLE

Structural Transition and Magnetic Property of $Bi_{1-x}Yb_xFeO_3$

Ya-nan Zheng[a], Yu-jie Wu[a,b*], Zhen-xing Qin[a], Xiao-jia Chen[a]

a. Department of Physics, South China University of Technology, Guangzhou 510640, China
b. School of Physics and Electronic Engineering, Guangzhou University, Guangzhou 510006, China

(Dated: Received on November 13, 2012; Accepted on February 1, 2013)

$Bi_{1-x}Yb_xFeO_3$($0\leq x\leq 0.2$) powders have been synthesized using a sol-gel method. The X-ray diffraction data show a structural transition from the rhombohedral R3c phase to the orthorhombic Pnma phase between x=0.1 and 0.125, which should induce a ferroelectric-paraelectric transformation. The phase transition is also proven by the Raman spectroscopy. A moderate signal on magnetization appears to illustrate the enhancement of magnetization at the transformation boundary, which is suggested to be the destruction of the spin cycloid structure at low concentration. The appearance of antiferromagnetic ordering is proposed to account for the afterward reduction of the magnetization at high concentration.

Key words: Multiferroics, Structural transition, Magnetic property

I. INTRODUCTION

Multiferroic materials can simultaneously exhibit ferroelectric/antiferroelectric, ferromagnetic/antiferromagnetic and/or ferroelastic ordering in a single phase. With these properties, they have promising potential in practical applications, such as multiple state memory elements, electronic field controlled ferromagnetic resonance devices, and so on [1−5]. Among these materials, $BiFeO_3$ with a distorted perovskite structure is one of the most extensively studied multiferroic materials. Its ferroelectricity transition temperature (T_C≈1103 K) [6] and antiferromagnetism Néel temperature (T_N≈640 K) [7] are above the room temperature, classing the compound a superiority to insight into the relation on aforementioned properties. This material has an antiferromagnetic G-type spin configuration where each Fe^{3+} is surrounded by six antiparallel nearest neighbors, and the antiferromagnetic axis rotates through the crystal with an incommensurate long-wavelength period of 620 Å [8]. In addition, the mechanism for the ferroelectricity essentially comes from the long range ordering of dipolar moments on Bi site, in relation with the existence of Bi lone pair and hybridization between Bi6s and O2p [9, 10]. However, two main problems hinder the practical applications, the first is the magnetoelectric effects cannot be observed in pure $BiFeO_3$ due to the space-modulated spin structure [11]. The other is a large leakage current density caused by charge defects in $BiFeO_3$. It is thus difficult to gain a well saturated ferroelectric hysteresis loop and a low dielectric loss [12−14]. Many attempts have been made to improve the ferroelectric property and derive ferromagnetic in the canted G-type antiferromagnetic order in $BiFeO_3$ [15−17]. It is well known that the doping process is one of the suitable methods to change the structure and properties of materials. Recently, many studies on the chemical substitutions have been undertaken. For instance, it has been established that rare earth (Re) ion substitution in the Bi site can reduce the leakage current [18−23]. Meanwhile, the dielectric ordering and magnetization can be improved as well.

The most common isovalent substitute in $BiFeO_3$ is La^{3+} for Bi^{3+}. La^{3+} has almost the same ionic radius as Bi^{3+} [24]. In order to obtain a more larger distortion, Sm^{3+}, Gd^{3+}, Ho^{3+}, and Y^{3+}, *etc.* are used to substitute at the Bi site. Polomska *et al.* observed that the appearance of the spontaneous magnetization induced by doping La^{3+} [25, 26], Gd^{3+} [27], and Sm^{3+} [28] in $BiFeO_3$. Bellakki *et al.* [29] and Minh *et al.* [30] reported the magnetization enhancement was a result of Y^{3+} doped in $BiFeO_3$. Wu *et al.* also reported that the remnant magnetization of $Bi_{1-x}Ho_xFeO_3$ was enhanced before approaching the ferroelectric-paraelectric phase boundary [31]. Although most of the Re ions have been chosen to be the dopants, there are only a few researches on the Yb^{3+} substitution. Yan *et al.* has reported that the electrical resistivity, ferroelectric and dielectric properties were improved by doping Yb^{3+} in $BiFeO_3$ [32]. Thaknria *et al.* studied the $Bi_{1-x}Yb_xFeO_3$ (x=0, 0.125), they observed the $Bi_{0.875}Yb_{0.125}FeO_3$ with the space group of Pbnm, and the magnetization of $Bi_{1-x}Yb_xFeO_3$ was enhanced when x=0.125 [33]. However, they only studied the properties of $BiFeO_3$ and $Bi_{0.875}Yb_{0.125}FeO_3$, the continuous change of cell parameters and magnetization of $Bi_{1-x}Yb_xFeO_3$ with the increasing of x were not discussed in detail. Additionally, whether the magnetization could be enhanced by doping Yb^{3+} in $BiFeO_3$,

*Author to whom correspondence should be addressed. E-mail: wyj9921@163.com, FAX: +86-20-39366871

when the value of x is higher than 0.125, has not been addressed until now. Yb^{3+} has a smaller ion radius ($\sim$1.2 Å) compared to most of the other Re ions, which is expected to improve more favorably the electrical and magnetic properties by doping Yb.

In this work, we present firstly the comprehensive properties of $Bi_{1-x}Yb_xFeO_3$($0\leq x\leq 0.2$) powders by X-ray diffraction (XRD), Raman and a physical property measurement system. We find a structural transition from the rhombohedral R3c to the orthorhombic Pnma, accompanying by a ferroelectric-paraelectric phase transition at x=0.1−0.125. The magnetization reaches the maximum at the ferroelectric-paraelectric phase boundary. The origin of the structural phase transition and ferroelectric-paraelectric phase transition, as well as the variation in magnetic behavior in $Bi_{1-x}Yb_xFeO_3$ powders are discussed in detail.

II. EXPERIMENTS

$Bi_{1-x}Yb_xFeO_3$ powders were prepared by a sol-gel method. Stoichiometric amounts of $Bi(NO_3)_3{\cdot}5H_2O$, $Yb(NO_3)_3{\cdot}5H_2O$, and $Fe(NO_3)_3{\cdot}9H_2O$ were dissolved in dilute nitric acid, the calculated amounts of tartaric acid were then added as a complexing agent. The resultant solution was dried at 150 °C with stirring to obtain xerogel powders. The dried xerogel powders were then grinded in an agate mortar. After that, the obtained powders were preheated to 300 °C for 1 h in order to get rid of excess hydrocarbons and NO_x impurities. All samples were annealed at 600 °C for 2 h. The phase purity and crystal structure characterization were done by an X-ray diffractometer with Cu Kα radiation. Raman scatting spectra were recorded by a Raman spectrometer (inVia Raman Microscope) in backscattering geometry. Magnetic measurements were carried out on a vibrating sample magnetometer in a physical property measurement system of Quantum Design.

III. RESULTS AND DISCUSSION

Figure 1 shows two selected XRD patterns ($Bi_{0.94}Yb_{0.06}FeO_3$ and $Bi_{0.825}Yb_{0.175}FeO_3$) corresponding to rhombohedral R3c phase and orthorhombic Pnma symmetry. Except for the $BiFeO_3$ and $Bi_{0.8}Yb_{0.2}FeO_3$, all samples have small impurities of $Bi_2Fe_4O_9$ which are probably attributed to the Fe rich phases. In order to have a better comprehending of the structural evolution of $Bi_{1-x}Yb_xFeO_3$, we have performed Rietveld refinements analysis on all samples using the FullProf program. The refined space groups are given with good agreement factor (R_p=9.79%, R_{wp}=9.85%, χ^2=2.78 for $Bi_{0.94}Yb_{0.06}FeO_3$, R_p=14.4%, R_{wp}=13.7%, χ^2=2.06 for $Bi_{0.825}Yb_{0.175}FeO_3$). The XRD patterns of the samples ($x\leq 0.1$) can be successfully refined in a rhombohedral symmetry. In the range

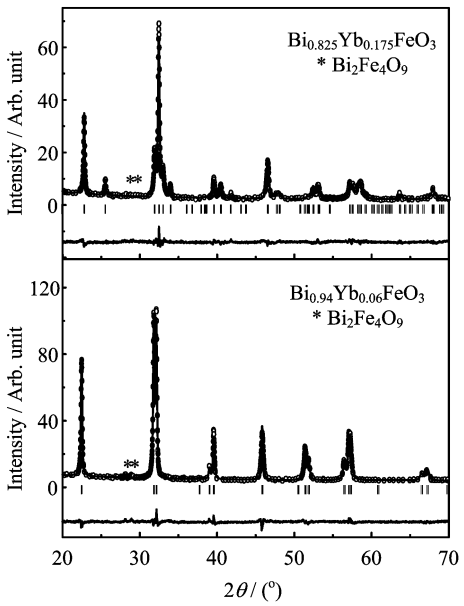

FIG. 1 XRD patterns of $Bi_{1-x}Yb_xFeO_3$ (x=0.06, 0.175) at room temperature. The symbol "*" represents the impurity $Bi_2Fe_4O_9$. The points represent the measured intensities and the lines represent the results of profile refinements. The positions of the Bragg reflections are marked by vertical lines and the difference profiles are shown at the bottoms.

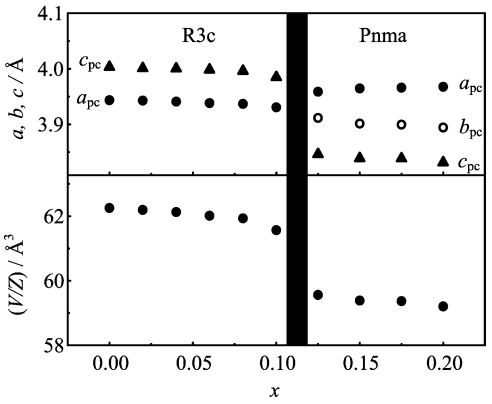

FIG. 2 The substitution x dependence of unit-cell volume V divided by the number of formula units per unit cell Z, the normalized lattice parameters of $Bi_{1-x}Yb_xFeO_3$ ($0\leq x\leq 0.20$). The cell parameters are described in a pseudocubic cell $a_{pc}=a/\sqrt{2}$, and $c_{pc}=c/2\sqrt{3}$ for the R3c phase, $a_{pc}=a/\sqrt{2}$, $b_{pc}=b/2$, and $c_{pc}=c/\sqrt{2}$ for the Pnma phase .

from 0.125 to 0.20, the samples are better described by the Pnma orthorhombic symmetry. It indicates that Yb doped $BiFeO_3$ undergoes the structural transition from the rhombohedral to the orthorhombic at the substitution concentration between x=0.10 and x=0.125.

We summarized the refined structural lattice parameters as a function of the concentration in Fig.2, expressed using a pseudocubic cell. The evolution of the lattice parameters again confesses us to the fact that the structural transition occurs at x=0.10−0.125. In the

DOI:10.1063/1674-0068/26/02/157-162

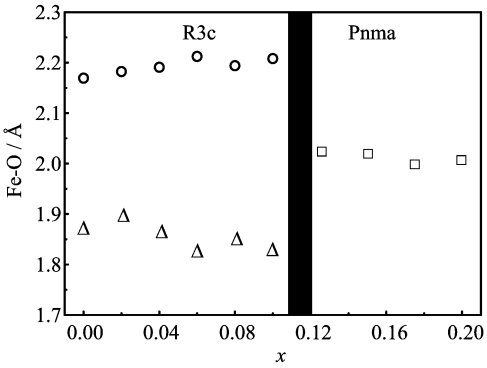

FIG. 3 The substitution x dependence of Fe−O bond lengths in the R3c and Pnma phases of $Bi_{1-x}Yb_xFeO_3$ ($0 \leq x \leq 0.20$).

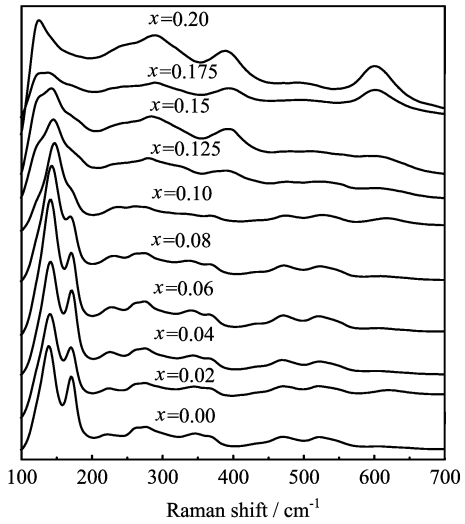

FIG. 4 Raman scattering spectra for $Bi_{1-x}Yb_xFeO_3$ ($0 \leq x \leq 0.20$) at room temperature.

range of $x \leq 0.10$, we can observe that a_{pc}, c_{pc}, and volume gradually decrease with the increasing concentration of Yb^{3+}, which is because the effective ionic radii of the trivalent ions with a coordination number of twelve get smaller upon the Yb doping. The abrupt decrease of b_{pc} and c_{pc} which results in a sudden decrease of volume at x=0.125, suggests the phase transition from the R3c rhombohedral phase to the Pnma orthorhombic phase between x=0.1 and x=0.125. $BiFeO_3$ is known to be the rhombohedral symmetry with space group R3c characterized by antiphase $a^-a^-a^-$ octahedral tilting and off-center ionic displacements along $[111]_c$ direction of pseudocubic. In the orthorhombic Pnma phase, it changes into nonpolar from polar corresponding to $a^-a^-a^+$ tilt system [34]. Moreover, the cell parameters and volume present an almost linear concentration dependent evolution.

The Fe−O bond lengths can be extracted from the Rietveld refinement analysis on all samples. The ferroelectric properties have a relative close relation with the Fe−O bond length [35]. It is worth to note that the Fe−O bond lengths change with the increasing concentration of Yb^{3+}. It is mentioned that $BiFeO_3$ is described by (i) rotations of adjacent oxygen FeO_6 octahedra around the [111] pseudocubic direction, which in turn gives rise to ferroelectricity, and (ii) Bi^{3+} and Fe^{3+} cations displace along the [111] threefold polar axis and off centered with respect to the bary center of the oxygen polyhedra, corresponding to ($a^-a^-a^-$) tilt system in Glazer's notation [36, 37]. Figure 3 displays the evolution of Fe−O bond lengths as a function of x. The octahedral bond environment in the R3c phase is comprised of three long degenerate Fe−O bond lengths and three short degenerate bond lengths. With increasing the concentration of Yb^{3+}, the three short and three long bond lengths in the R3c symmetry become six equal bond lengths in the orthorhombic Pnma phase. And the observed change of the Fe−O bond length is the evidence of displacement of Fe^{3+}. It also indicates that the structure symmetry of $BiFeO_3$ has changed into paraelectric from ferroelectric accompanying with the rhombohedral R3c-orthorhombic Pnma phase transition.

Raman scattering spectra are used to study the vibrational properties of $BiFeO_3$. Valuable information can be obtained by fitting the Raman spectra, such as the frequency of each mode, the peak position of each component. Figure 4 shows the Raman scattering spectra of all samples at room temperature. According to the factor group analysis, there are 13 Raman active modes of the rhombohedral with the space group R3c. They can be summarized by the following irreducible representation: $\Gamma_{Raman}=4A_1+9E$. For the pure $BiFeO_3$, three sharp peaks at around 138, 175, and 220 cm^{-1} are assigned as A_1 modes. A_1-4 and E-1 modes at around 432 and 124 cm^{-1} have quite weak scattering intensities, and eight weak peaks at 260, 277, 303, 345, 368, 470, 523, and 622 cm^{-1} are assigned as other E modes.

From a vibrational point of view, low frequency modes can be attributed as external modes result from the relative motion of Bi^{3+} cations against the oxygen octahedrons [17]. For the compounds $Bi_{1-x}Yb_xFeO_3$ (x=0−0.1), the A_1 modes at 138, 170, and 223 cm^{-1} and E modes at 124 and 260 cm^{-1} are related to the Bi−O covalent bonds [38]. From Fig.4, when x=0−0.1, we can see that the five modes which are related to the Bi−O bonds are broadened and the intensities of the modes at 138, 170, 223, and 260 cm^{-1} get weaker gradually with increasing x, the above changes can be attributed to the decrease of the percent of the Bi−O bonds due to the Bi ion substituted by Yb ion. However, the Bi−O covalent bonds and noncentrosymmetric ferroelectric distortion remain quite stable, thus the $Bi_{1-x}Yb_xFeO_3$ samples maintain the rhombohedral R3c phase in the range of $0 \leq x \leq 0.1$. When x=0.1−0.125, the intensity of the mode at 124 cm^{-1} abruptly increases while the intensities of

DOI:10.1063/1674-0068/26/02/157-162

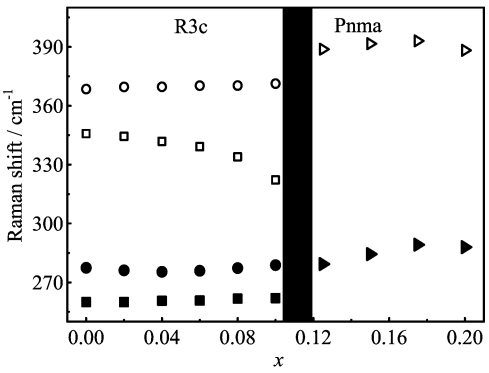

FIG. 5 The substitution x dependence of the frequencies for the selected Raman modes of the $Bi_{1-x}Yb_xFeO_3$ rhombohedral and orthorhombic phases.

other modes suddenly become weaker, which should be regarded as the faster change of the Bi−O covalent bonds near the ferroelectric-paraelectric transition. When $x\geq0.125$, there should be 24 Raman-active modes ($7A_g+5B_{1g}+7B_{2g}+5B_{3g}$) for the orthorhombic Pnma phase. However, we can only obtain 11 modes in Pnma phase which is due to the unpolarized feature in our instrument, and the number of unpolarized Raman-active modes is about half that of the polarized ones in Pnma orthorhombic structure. This phenomenon was also observed in $LaMnO_3$ [39].

In order to further confirm the phase transition, we fitted all the modes by Lorentz fitting. The evolution of the frequency of four selected modes (at 260, 277, 345, and 368 cm^{-1}, respectively) as a function of x is presented in Fig.5. With increasing x, it can be seen that the noncentrosymmetry E modes at 260 and 277 cm^{-1} shift progressively to 279 cm^{-1} at x=0.125 while the frequency of E mode at 368 cm^{-1} increases abruptly at x=0.125. At the same time, the mode at 345 cm^{-1} shifts to lower frequency and then disappears when $x\geq0.125$. The evolution of the four Raman modes also reveals that the structural transition from R3c to Pnma takes place at x=0.10−0.125. The results based on the Raman spectra are consistent with the results of XRD.

Figure 6 shows the magnetic hysteresis loops of $Bi_{1-x}Yb_xFeO_3$ (x=0, 0.06, 0.10, and 0.15) with a maximum field of 9.0 T at room temperature. All loops are not saturated. It is indicated the antiferromagnetic structure with the spiral magnetic ordering in these $Bi_{1-x}Yb_xFeO_3$ [40−43]. $BiFeO_3$ has a G-type magnetic order and a canted spin structure giving a spiral modulation with a periodicity of 62 nm. And Fe magnetic moments are coupled antiferromagnetically between adjacent planes and ferromagnetically within the pseudocubic plane. It has been reported that the G-type magnetic structure can be modified by subjecting it to a long range modulation by the cycloid spiral with the $[110]_H$ spiral direction and $(110)_H$ spin rotation plane [44]. From Fig.6, we observe that the pure $BiFeO_3$ has

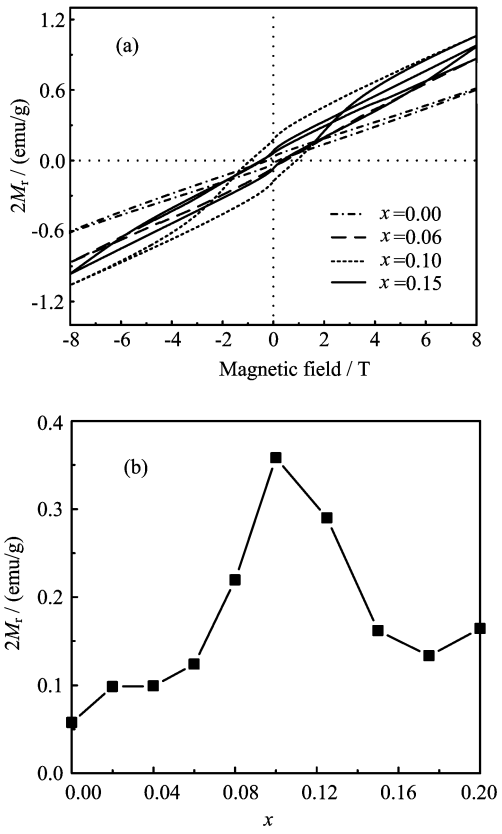

FIG. 6 (a) Magnetic field dependence of the magnetization obtained for $Bi_{1-x}Yb_xFeO_3$ samples at room temperature. (b) Two times the remnant magnetization ($2M_r$) as a function of the Yb concentration x.

a very low value of remnant magnetization. The hysteresis loop is almost linear. Moreover, the magnetization is enhanced with increasing the concentration of Yb as expected. The similar results have been obtained in other Re-substituted $BiFeO_3$ such as $Bi_{1-x}Sm_xFeO_3$ [14], $Bi_{1-x}Ho_xFeO_3$ [13, 17], and $Bi_{1-x}La_xFeO_3$ [21]. Since the $Bi_2Fe_4O_9$ is paramagnetic at room temperature [11], and the amount of impurity ($Bi_2Fe_4O_9$) phase is about 5%, which almost has no effect on the magnetic property of $BiFeO_3$. When the value of x is lower than 0.1, the magnetization is gradually enhanced with the increasing of Yb concentration. This behavior may be due to that the periodicity of the spiral magnetic spin structure increases with the increasing of the Yb substitution, according to the neutron diffraction experiments [45, 46]. The spin cycloid structure continues to be destructed as the Yb substitution increases. That is to say, the Yb substitution can only suppress but cannot destroy the spin cycloid structure completely as the substituted concentration is below 0.1. When x=0.1, the magnetization reaches the maximum, indicating that the spin spiral is completely broken. However, the magnetization begins to decrease as the continual increasing of the Yb concentration.

In order to further understand the magnetic prop-

DOI:10.1063/1674-0068/26/02/157-162

erty of the $Bi_{1-x}Yb_xFeO_3$, we plot the $2M_r$ values as a function of x in Fig.6(b). We note that in the region of x<0.1, the $2M_r$ increases as increasing x. Then $2M_r$ reaches the maximum at x=0.1 which is around the point of ferroelectric-paraelectric phase transition. This indicates that complete removal of the cycloid-type spin modulation at x=0.1 and the latent magnetization is released. However, the $2M_r$ starts to decline when $x\geq$0.125. The similar phenomenon was also observed that the helical spin structure of $BiFeO_3$ was modified towards a collinear antiferromagnetic structure beyond x=0.2 concentration [45], and the spin modulated spin structure was gradually prevented by La or Mn doping [46]. The decrease of magnetization for $x\geq$0.125 originates from the appearance of perfect antiferromagnetic ordering in the orthorhombic structure in $Bi_{1-x}Yb_xFeO_3$. Moreover, doping $BiFeO_3$ with the Yb stabilizes the collinear antiferromagnetic, and the space modulated spin structure is gradually prevented by Yb doping.

IV. CONCLUSION

$Bi_{1-x}Yb_xFeO_3$ powders have been prepared successfully by a sol-gel method. Through the investigation on the structural, vibrational and magnetic properties, we find that the phase transition from rhombohedral R3c symmetry to orthorhombic Pnma phase occurs at x=0.1−0.125 accompanying with the ferroelectric-paraelectric phase transition. In the range of $x\leq$0.10, the magnetization increases with the increasing of x. This increase results from the destruction of the spin cycloid and the release of the locked magnetization. Moreover, the maximum magnetization is just at the ferroelectric-paraelectric phase boundary, which is reasonable that the structural phase transition completely break the spin cycloid structure and the latent magnetization is entirely released. When $x\geq$0.125, the magnetization decreases as x continues to increase, suggesting the appearance of perfect antiferromagnetic ordering in the orthorhombic structure.

V. ACKNOWLEDGMENTS

This work was supported by the Cultivation Fund of the Key Scientific and Technical Innovation Project, the Ministry of Education of China (No.708070), the National Natural Science Foundation of China (No.10874046 and No.11104081), and the Fundamental Research Funds for the Central Universities (No.2012zz0078).

[1] W. Eerenstein, N. D. Mathur, and J. F. Scott, Nature **442**, 759 (2006).
[2] M. Fiebig, J. Phys. D **38**, R123 (2005).
[3] J. Wang, J. B. Neaton, H. Zheng, V. Nagarajan, S. B. Ogale, B. Liu, D. Viehland, V. Vaithyanathan, D. G. Schlom, U. V. Waghmare, N. A. Spaldin, K. M. Rabe, M. Wuttig, and R. Ramesh, Science **299**, 1719 (2003).
[4] S. Dong, J. F. Li, and D. Viehland, Appl. Phys. Lett. **83**, 2265 (2003).
[5] S. Dong, J. Zhai, J. F. Li, D. Viehland, and M. I. Bichurin, Appl. Phys. Lett. **89**, 243512 (2006).
[6] J. R. Teague, R. Gerson, and W. J. James, Solid State Commun. **8**, 1073 (1970).
[7] P. Fischer, M. Polomska, I. Sosnowska, and M. Szymanski, J. Phys. C **13**, 1931 (1980).
[8] I. Sosnowska, T. P. Neumaier, and E. Steichele, J. Phys. C **15**, 4835 (1982).
[9] N. A. Hill, J. Phys. Chem. B **104**, 6694 (2000).
[10] R. Rai, S. K. Mishra, N. K. Singh, S. Sharma, and A. L. Kholkin, Curr. Appl. Phys. **11**, 508 (2011).
[11] Y. H. Lin, Q. H. Jiang, Y. Wang, and C. W. Nan, Appl. Phys. Lett. **90**, 172507 (2007).
[12] A. K. Pradhan, K. Zhang, D. Hunter, J. B. Dadson, G. B. Loutts, P. Bhattacharya, R. S. Katiyar, J. Zhang, D. J. Sellmyer, U. N. Roy, Y. Cui, and A. Burger, J. Appl. Phys. **9**, 093903 (2005).
[13] Y. P. Wang, L. Zhou, M. F. Zhang, X. Y. Chen, J. M. Liu, and Z. G. Liu, Appl. Phys. Lett. **84**, 1731 (2004).
[14] M. M. Kumar, V. R. Palkar, K. Srinivas, and S. V. Suryanarayana, Appl. Phys. Lett. **76**, 2764 (2000).
[15] Y. J. Zhang, H. G. Zhang, J. H. Yin, H. W. Zhang, J. L. Chen, W. Q. Wang, and G. H. Wu, J. Magn. Magn. Mater. **322**, 2251 (2010).
[16] G. L. Yuan, S. W. Or, J. M. Liu, and Z. G. Liu, Appl. Phys. Lett. **89**, 052905 (2006).
[17] F. Bai, J. Wang, M. Wuttig, J. Li, N. Wang, A. P. Pyatakov, A. K. Zvezdin, L. E. Cross, and D. Viehland, Appl. Phys. Lett. **86**, 032511 (2005).
[18] Z. X. Cheng, A. H. Li, X. L.Wang, S. X. Dou, K. Ozawa, H. Kimura, S. J. Zhang, and T. R. Shrout, J. Appl. Phys. **103**, 07E507 (2008).
[19] V. A. Khomchenko, D. A. Kiselev, E. K. Selezneva, J. M. Vieira, A. M. L. Lopes, Y. G. Pogorelov, J. P. Araujo, and A. L. Kholkin, Mater. Lett. **62**, 1927 (2008).
[20] P. Uniyal and K. L. Yadav, Mater. Lett. **62**, 2858 (2008).
[21] S. T. Zhang, Y. Zhang, M. H. Lu, C. L. Du, Y. F. Chen, Z. G. Liu, Y. Y. Zhu, N. B. Ming, and X. Q. Pan, Appl. Phys. Lett. **88**, 162901 (2006).
[22] Y. J. Wu, X. K. Chen, J. Zhang, and X. J. Chen, J. Appl. Phys. **111**, 053927 (2012).
[23] Y. J. Wu, X. K. Chen, J. Zhang, and X. J. Chen, J. Magn. Magn. Mater. **324**, 1348 (2012).
[24] R. D. Shannon, Acta Crystallogr. Sect. A **32**, 751 (1976).
[25] M. Polomska, W. Kaczmarek, and Z. Pajak, Phys. Status Solidi **23**, 567 (1974).
[26] M. Polomska and W. Kaczmarek, Acta Phys. Pol. A **45**, 199 (1974).
[27] V. A. Khomchenko, D. A. Kiselev, I. K. Bdikin, V. V. Shvartsman, P. Borisov, W. Kleemann, J. M. Vieira, and A. L. Kholkin, Appl. Phys. Lett. **93**, 262905 (2008).
[28] V. A . Khomchenko, J. A. Paixao, V. V. Shvartsman, P. Borisov, W. Kleemann, D. V. Karpinsky, and A. L.

DOI:10.1063/1674-0068/26/02/157-162

Kholkin, Scripta Mater. **62**, 238 (2010).
[29] M. B. Bellakki and V. Manivannan, J. Sol-Gel Sci. Technol. **53**, 184 (2010).
[30] N. V. Minh and D. V. Thang, J. Alloys Compd. **505**, 619 (2010).
[31] Y. J. Wu, J. Zhang, X. K. Chen, and X. J. Chen, Solid State Commun. **151**, 1936 (2011).
[32] Z. Yan, K. F. Wang, J. F. Qu, and Y. Wang, Appl. Phys. Lett. **91**, 082906 (2007).
[33] P. Thakuria and P. A. Joy, Appl. Phys. Lett. **97**, 162504 (2010).
[34] I. Levin, S. Karimi, V. Provenzano, C. L. Dennis, H. Wu, T. P. Comyn, T. J. Stevenson, R. I. Smith, and I. M. Reaney, Phys. Rev. B **81**, 020103R (2010).
[35] D. C. Arnold, K. S. Knight, F. D. Morrison, and P. Lightfoot, Phys. Rev. Lett. **102**, 027602 (2009).
[36] A. M. Glazer, Acta Crystallogr. Sect. B **28**, 3384 (1972).
[37] R. Haumont, I. A. Kornev, S. Lisenkov, L. Bellaiche, J. Kreisel, and B. Dkhil, Phys. Rev. B **78**, 134108 (2008).
[38] G. L. Yuan, S. W. Or, and H. L. W. Chan, J. Appl. Phys. **101**, 064101 (2007).
[39] M. N. IIiev, M. V. Abrashev, H. G. Lee, V. N. Popov, Y. Y. Sun, C. Thomsen, R. L. Meng, and C. W. Chu, Phys. Rev. B **57**, 2872 (1998).
[40] G. L. Yuan and S. W. Or, J. Appl. Phys. **100**, 024109 (2006).
[41] R. K. Mishra, D. K. Pradhan, R. N. P.Choudhary, and A. Banerjee, J. Magn. Magn. Mater. **320**, 2602 (2008).
[42] S. T. Zhang, M. H. Lu, D. Wu, Y. F. Chen, and N. B. Ming, Appl. Phys. Lett. **87**, 262907 (2005).
[43] A. A. Amirov, I. K. Kamilov, A. B. Batdalov, I. A. Verbenko, O. N. Razumovskaya, L. A. Reznichenko, and L. A. Shilkina, Tech. Phys. Lett. **34**, 760 (2008).
[44] M. M. Kumar, S. Srunath, G. S. Kummar, and S. V. Suryanarayana, J. Magn. Magn. Mater. **188**, 203 (1998).
[45] I. Sosnowska, W. Schäfer, W. Kockelmann, K. H. Andersen, and I. O. Troyanchuk, Appl. Phys. A **74**, S1040 (2002).
[46] I. Sosnowska, M. Loewenhaupt, W. I. F. David, and R. M. Ibberson, Mater. Sci. Forum **683**, 133 (1993).

DOI:10.1063/1674-0068/26/02/157-162